IEEE Access
Multidisciplinary ⋮ Rapid Review ⋮ Open Access Journal

Received 31 January 2024, accepted 17 March 2024, date of publication 25 March 2024, date of current version 29 March 2024.

Digital Object Identifier 10.1109/ACCESS.2024.3380023

RESEARCH ARTICLE

A Comparative Study of Estimating Hourly Images of MODIS Land Surface Temperature Using Diurnal Temperature Cycle Models in Arid Regions

FAHIME ARABI ALIABAD[1], EBRAHIM GHADERPOUR[2], MOHAMMAD ZARE[3], AND HAMIDREZA GHAFARIAN MALAMIRI[1]

[1]Department of Remote Sensing, Yazd University, Yazd 8915818411, Iran
[2]Department of Earth Sciences, Sapienza University of Rome, 00185 Rome, Italy
[3]Department of Arid Lands Management, Yazd University, Yazd 8915818411, Iran

Corresponding author: Ebrahim Ghaderpour (ebrahim.ghaderpour@uniroma1.it)

This work was supported in part by the Sapienza University of Rome.

ABSTRACT Thermal monitoring of different regions is usually limited to meteorological data in ground stations. Meteorological networks are limited in arid and semi-arid areas, where monitoring climatic conditions is not possible. The aim of this study is to estimate the land surface temperature (LST) hourly for Yazd-Ardakan plain by modeling the diurnal temperature cycle (DTC) using LST imagery of moderate resolution imaging spectroradiometer (MODIS). First, MODIS imagery are reconstructed using the multi-channel singular spectrum analysis, and the complete time series without missing values are created. Then, six DTC models are compared. The accuracy of DTC models is examined by ground LST measurements, air temperature, humidity, and wind speed. In addition, the results of examining the root mean square error (RMSE) images obtained from cross-validation based on MODIS LST imagery show that DTC2 has the highest error, where 73% of the area has RMSE greater than 3°C. In DTC1 and DTC2, 64% and 5.8% of the study region has RMSE less than 2°C. In general, DTC1, DTC6, DTC5, DTC4, DTC3, and DTC2 models have shown the highest to lowest accuracy in modeling the LST diurnal cycle. In addition, the difference between LST in mountain and plain lands is greater at the time of maximum temperature than at other hours of the day and night. The findings of this research are crucial in studies concerning climate change and land environmental monitoring in arid/semi-arid regions.

INDEX TERMS Arid land, diurnal temperature cycle, land surface temperature, MODIS, thermal remote sensing.

I. INTRODUCTION

Land surface temperature (LST), an important parameter in the Earth's climate system, affects the exchange of matter and energy between the Earth and the atmosphere on a regional and global scale [1], [2], [3], [4], [5]. LST diurnal cycle changes are related to atmospheric conditions, solar radiation, soil thermal regime and vegetation cover [6], [7], [8], [9]. LST diurnal cycle has applications in urban thermal environment monitoring, thermal inertia, energy balance, evaporation, transpiration, and others [10], [11], [12], [13], [14], [15], [16]. In many models associated with energy and temperature exchange, hourly surface temperature data are required [11]. Certain remote sensing satellites provide a unique tool to measure the radiation of the thermal wavelengths of the electromagnetic curve, which can be used to calculate LST with different time resolution [17]. However, except for Geostationary satellites that have the ability to measure hourly temperature, the rest of the satellites that have a thermal band do not have this feature [18], [19], [20].

The moderate resolution imaging spectroradiometer (MODIS) sensor was launched in 1999 aboard the Terra satellite and in 2002 aboard the Aqua satellite [21], [22]. Both platforms have been acquiring data in 36 spectral bands [23].

The associate editor coordinating the review of this manuscript and approving it for publication was Jon Atli Benediktsson.

Terra and Aqua satellites have daily time resolution, and each one measures LST twice a day [24], [25], [26]. The MODIS sensor has a wide spectral range used in various studies [27], [28], [29]. Its bands 31 and 32 are used to estimate LST [30], [31].

In thermal remote sensing, a method has been presented for modeling the LST diurnal cycle [32]. Some studies have already been conducted to estimate the hourly temperature by modeling the diurnal temperature cycle (DTC) [33], [34], [35], [36], [37]. The results of studies by Göttsche and Olesen showed that by modeling DTC using METEOSAT data, it is possible to estimate the temperature with a 30-minute sequence [38]. Coops et al. estimated LST in the morning from 2000 to 2002, when the Aqua satellite was not yet launched [39]. Their results showed that LST obtained from the Terra satellite in the afternoon can be used to predict more than 90% of LST in the morning.

Duan et al. evaluated six models of LST diurnal cycle using satellite images in cloudless sky [40]. They considered two time periods: one for the whole day, i.e., from sunrise to sunrise (Period A) and another from 09:00 AM to 03:00 AM of the next day in local time (Period B). The results of period A showed that JNG06 and GOT09 models performed best with root mean square error (RMSE) of 0.5°C. The GOT01_0 model performed the worst with an overall RMSE of 1°C. The results of period B showed that except for the GOT01_0 model, other models had similar results with an overall RMSE of 0.4°C.

Holmes et al. investigated the spatial patterns in the timing of the LST diurnal cycle [41]. In fact, the structural differences in the timing of DTC, caused by the choice of measurement device or model framework, were examined. Duan et al. estimated DTC at high spatial and temporal resolution using MODIS products and evaluated with LSTs derived from MSG-SEVIRI [42]. Their results achieved RMSE smaller than 1°C. Results of the study conducted by Malbeteau et al. showed that the unmanned aerial vehicle (UAV)-based diurnal cycle was consistent with ground measurements with an average correlation coefficient and RMSE of 0.99°C and 0.68°C, respectively [43]. Nie et al. simulated DTC using MODIS imagery [44]. Their results showed that RMSE in eight validation points in different land covers was smaller than 0.72°C. They validated their results by comparing the simulated LST of MODIS products with FY-2F. Chang et al. evaluated 4-parameter DTC models using MODIS LST images and ground measurements [45]. All models had higher accuracy in summer than other seasons, while poorer performance was produced in winter. The INA08-ts model showed the best performance in all seasons. Sharifnezhadazizi et al. analyzed the global DTC using MODIS observations [46]. Preliminary evaluation of LST interpolated with hourly ground observations showed an error of less than 1°C.

Sekertekin et al. modeled diurnal LST in arid regions using artificial neural network and Landsat 8 image time series [47]. Their results showed that the difference between the estimated surface temperature and the ground data was 1°C in winter and 2.49°C in summer, and the accuracy of this model decreases with increasing temperature. Hu et al. improved the monthly LST estimation of the MODIS sensor using the diurnal cycle model of LST [48]. This method has made it possible to estimate the average and maximum temperature of 24 hours in a diurnal cycle in every month. Validation of the mean temperature based on DTC estimated the mean difference compared to the ground data of 0.3°C with RMSE of 2.2°C.

Xing et al. estimated the daily average LST on a global scale using pairs of observations from the MODIS sensor during day and night [49]. Their RMSE results showed less than 1.06°C. Sismanidis et al. quantified the daily and annual dynamics of LST obtained from satellites and stated that the Earth's diurnal and annual cycles drive the changes of LST in space and time, but their combined effects are transferred differently from place to place as a function of weather, local weather conditions, and surface characteristics [50]. Lu and Zhou presented a 4-parameter model to estimate the LST diurnal cycle using MODIS LST [51]. They showed that their model can record the changes of LST during a day very well. Jia et al. estimated the hourly product of LST with a spatial resolution of 2 km using advanced baseline imager (ABI) data [52]. Compared to the value obtained from the hourly data, the daily average of LST showed RMSE of 1.13°C and the correlation coefficient of 0.99. Hong et al. generated, validated, and analyzed a global dataset of daily mean LST without missing data using MODIS products [53]. Validation using terrestrial data showed that the mean absolute errors (MAEs) in the IADTC framework were 1.4°C for the SURFRAD data and 1.1°C for the FLUXNET data.

Thermal monitoring of different regions is usually restricted to meteorological data in ground stations [5], [54], [55]. There are few meteorological networks in arid and semi-arid areas, and it is not possible to monitor climatic conditions, especially on a regional and local scale, in these environments [56]. Therefore, the aim of the current research is to estimate the LST images on an hourly basis using the DTC modeling. Deriving LST images with hourly sequence has wide applications in monitoring energy balance and soil thermal properties. The rest of this study is organized as follows. Section II describes the study area, employed data sets, and DTC models from MODIS LST measurements. Results and discussion are presented in Section III, and conclusions, recommendations, and future directions are provided in Section IV.

II. MATERIALS AND METHODS

A. STUDY REGION

The study region is Yazd-Ardakan plain, located in Yazd province in the center of Iran (Fig. 1). This region has desert conditions and a hot and arid climate. Rainfall is very little and irregular, with a long-term annual average of 60 mm. This region is selected for the DTC modeling due to its desert

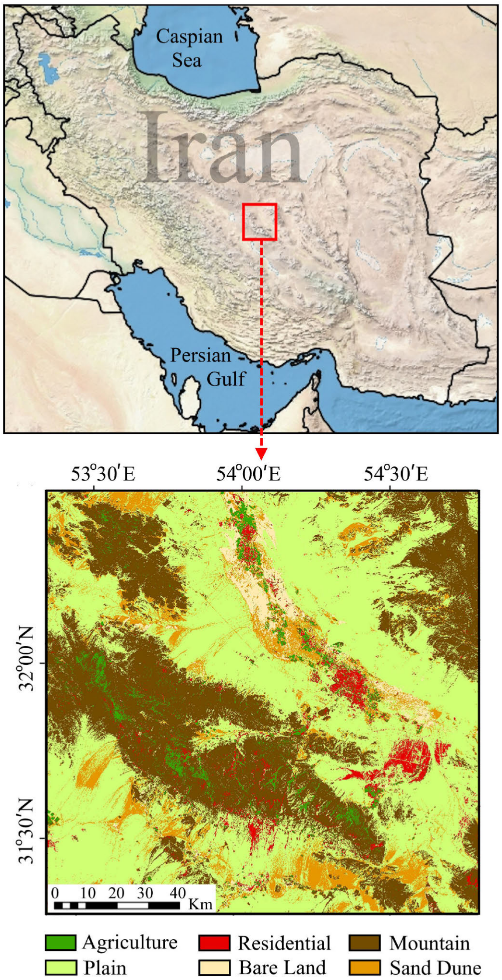

FIGURE 1. **The Yazd-Ardakan plain in the province of Yazd in Iran.**

nature and the sharp increase in air and land temperatures in summer.

B. DATASETS AND PREPROCESSING

The MODIS LST is estimated using a generalized split window algorithm. This algorithm is similar to the split window method presented by [57] and [58] for AVHRR data based on the day and night physics developed in [59]. In this method, LST is derived using classification-based emissivity [60]. These two polar orbiting satellites carry out imaging with daytime resolution of about 10:30 AM/PM local solar time for Terra and 1:30 AM/PM for Aqua [61], [62], freely available as MOD11A1 and MYD11A1 [63]. Herein, MODIS LST images are employed with a sequence of four times per day in all days of 2020 that includes a total of 1460 images. All these images are reconstructed using the multi-channel singular spectrum analysis (MSSA) to create a time series without missing data and outliers for modeling the LST cycle. The reconstruction of these images using MSSA is described in detail in [64]. The MSSA is a robust time series analysis model that simultaneously accounts for the temporal and spatial correlations between multiple time series. More details on how MSSA is applied to reconstruct LST images can be found in [64] and [65]. The six DTC models mentioned below (DTC1-DTC6) are compared. Ground data as well as MODIS images are employed for validation. After selecting the optimal method, LST is modeled hourly in every day and night. Annual LST time series is created with hourly sequence (8760 images for one year). The steps of modeling the diurnal cycle of LST using MODIS imagery are illustrated in Fig. 2. Note that the labels ‘A’ to ‘H’ in red in Fig. 2 are the same as the labels of the subsections in Section III to ease understanding.

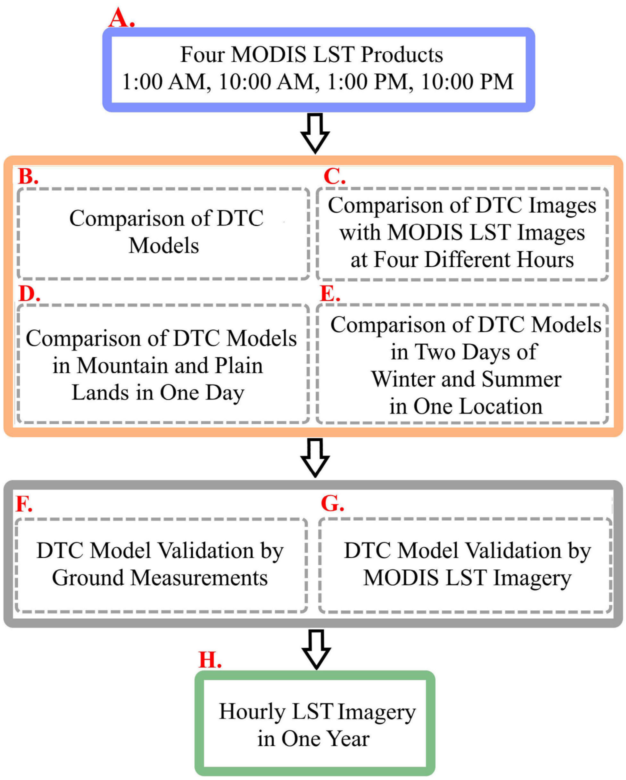

FIGURE 2. **The workflow of this study.**

C. DIURNAL TEMPERATURE CYCLE MODELS

To estimate LST with hourly sequence, a model consisting of a harmonic and an exponential term is fitted to the Earth’s DTC model, which describe the effect of the sun and the reduction of LST at night, respectively [66], [67], [68]. Modeling estimates the parameters that describe DTC and can also be useful for interpolating missing data due to technical or cloud problems [69], [70]. The parameters depend on all modeled temperatures and are therefore hardly affected by outliers [71].

1) DTC1

A two-part, semi-empirical DTC model is developed in [38]. The LST cycle is modeled using the cosine function to predict the evolution of LST during the day and based on the thermal diffusion equation and an exponential function to describe the temperature decrease at night, assuming that natural surfaces follow Newton's law of cooling [72]. In the present study, this model is called DTC1 and is defined as

$$T_{\text{day}}(t) = T_0 + T_a \cos\left(\frac{\pi}{w}(t - t_m)\right), \quad t < t_s \tag{1}$$

$$T_{\text{night}}(t) = T_0 + \delta_T + \left[T_a \cos\left(\frac{\pi}{w}(t_s - t_m)\right) - \delta_T\right] \times \exp\left(\frac{t_s - t}{k}\right), \ t_s \le t \tag{2}$$

where k is the temperature decrease constant given by the following equation,

$$k = \frac{w}{\pi}\left[\tan^{-1}\left(\frac{\pi}{w}(t_s - t_m)\right) - \frac{\delta_T}{T_a}\sin^{-1}\left(\frac{\pi}{w}(t_s - t_m)\right)\right]. \tag{3}$$

All the parameters of these equations are also ilustrated in [40, Figure 1]. Here, t denotes the time, T_0 is the residual surface temperature around sunrise, T_a is the range of surface temperature in one day and night, w is the width in half of the period (considered as the length of the day), t_m is the time in which the surface temperature reaches its maximum in 24 hours, t_s is the starting time of the temperature decrease after sunset, δ_T is the temperature difference between the lowest temperature and T_0. In this model, clear sky conditions are assumed (non-cloudy pixels) without any significant change in wind speed and temperature drop after the thermal sunset defined by t_s.

The components of the time of sunrise and sunset, the length of the day and the local noon (when the sun has the most amount of radiation) are calculated using the geographical location of the study region and the day of the year for each day of the year to estimate t_s, t_m, and w. The length of the day, w, also called the maximum possible sunshine hours, is defined as the time between sunrise and sunset [73]:

$$w = \frac{2}{15}\cos^{-1}\left(-\tan\delta\tan\phi\right) \tag{4}$$

where δ is the solar declination angle in degrees and ϕ is the latitude of the region in degrees. A suitable approximate equation for calculating the solar declination using the day of the year, D_n, is presented by Cooper [74] as follows

$$\delta = 23.45\sin\left((360/365)(284 + D_n)\right). \tag{5}$$

The time of sunrise, t_{sr}, and the time of sunset, t_{ss}, can be calculated with the location's latitude (ϕ degrees) and solar declination (δ degrees) as

$$t_{\text{sr}} = 12 - (12/\pi)\cos^{-1}\left(\tan(\phi)\tan(\delta)\right) \tag{6}$$

$$t_{\text{ss}} = 12 + (12/\pi)\cos^{-1}\left(\tan(\phi)\tan(\delta)\right) \tag{7}$$

The local solar time, when the sun is at the highest level of the sky, is used to calculate the time of maximum temperature, t_m. The solar time, defined based on the daily apparent movement of the sun around the Earth, is the hourly angle of the sun relative to the observer's meridian. The local solar time is the sum of local time and the time correction (TC) factor. The local time usually differs from the local solar time because of eccentricity of the Earth's orbit and as a result of human adjustments for summer savings. The TC or net time correction factor (in minutes) calculates the local solar time changes in a given time zone due to longitude changes in the time zone:

$$\text{TC} = 4\left(\text{Longitude} - 15\delta_{T_{\text{UTC}}}\right) - \text{E}_0\text{T} \tag{8}$$

Here, the coefficient 4 minutes is because the Earth rotates one degree every 4 minutes, E_0T stands for equation of time, and $\delta_{T_{\text{UTC}}}$ is the difference between the local time and the universal coordinated time (UTC) in hours, which is 3.5 hr in the study region. The E_0T is an empirical equation that corrects for Earth's orbital eccentricity and Earth's axial tilt, approximately equal to

$$\text{E}_0\text{T} = 9.87\sin(2B) - 7.53\cos(B) - 1.5\sin(B), \tag{9}$$

where $B = (360/365)(d - 81)$ and d is the number of days that have passed since the beginning of the year.

2) DTC2

In the diurnal cycle model of LST developed by Schädlich et al. [75], δ_T in Eqs. (2) and (3) is considered zero. Herein, this method is called DTC2.

3) DTC3

Van den Bergh et al. found that the width of the best fitted cosine term of the DTC is different on the upslope (morning) than on the downslope (afternoon) [76]. As a result, they proposed a DTC model in which an additional term is introduced based on previous models. The whole DTC is represented by three functions, which represent two curve functions during the day, one for the upslope and the other for the downslope, while the third term describes the shape of the nocturnal curve. This model, DTC3, is defined as:

$$T_{\text{day1}}(t) = T_0 + T_a \cos\left(\frac{\pi}{w}(t - t_m)\right), \quad t < t_m \tag{10}$$

$$T_{\text{day2}}(t) = T_0 + T_a \cos\left(\frac{\pi}{w_2}(t - t_m)\right), \quad t_m \le t < t_s \tag{11}$$

$$T_{\text{night}}(t) = T_0 + T_a \cos\left(\frac{\pi}{w_2}(t_s - t_m)\right) \times \exp\left(\frac{t_s - t}{k}\right), \quad t \ge t_s \tag{12}$$

where $w_2 = 3.4\ t_m$ and k is calculated as

$$k = \frac{w_2}{\pi}\tan^{-1}\left(\frac{\pi}{w_2}(t_s - t_m)\right). \tag{13}$$

4) DTC4

Another model presented by Inamdar et al. uses a pseudo-hyperbolic function to replace the exponential function in DTC1 [77]. More precisely, $\exp\left((t_s - t)/k\right)$ in Eq. (2) is replaced by $k/\left(k + t - t_s\right)$, and the new model is called DTC4 in the present study.

5) DTC5

Duan et al. [42] optimized the LST cycle model presented by Inamdar et al. [77]. Duan et al. reduced the width, w, greater than half a period in the cosine term of the thermal diffusion equation. The equation for estimating day and night temperature in this model, named hereafter DTC5, is identical to DTC4, but only the method of estimating w component is different, estimated using the following equation:

$$w = (4/3)\left(t_m - t_s\right) \tag{14}$$

6) DTC6

Hu et al. proposed a different way for calculating the day and night LST parameters [48]. This method, named DTC6 hereafter, uses the same equations for calculating T_{day} and T_{night} as DTC5, but k, T_0, T_a, and δ_T are calculated by the following equations.

$$k = \frac{T_a \cos(u) - \delta_T}{(\pi T_a/w)\sin(u)} \tag{15}$$

where $u = (\pi/w)(t_s - t_m)$ and $w = (4/3)t_m$. Furthermore,

$$T_a = \frac{T_{\max} - T_{\text{sr},d}}{\cos(\pi/4) + 1} \tag{16}$$

$$T_0 = T_{\text{sr},d} + T_a \cos(\pi/4) \tag{17}$$

$$\delta_T = \frac{T_a\Big(\cos(u)\big(T_a\cos(u) + D\big) + DS\Big)}{D - T_a\big(S - \cos(u)\big)} \tag{18}$$

where $S = (\pi/4)\sin(u)(24 - t_s)$ and $D = T_0 - T_{\text{sr},d+1}$. In these equations, $T_{\text{sr},d}$ is LST at the time of sunrise on the first day, and $T_{\text{sr},d+1}$ is LST at the time of sunrise of the next day whose images are estimated using the mean and range. Also, $T_{\max}$ is the maximum day and night LST at time t_m.

III. RESULTS AND DISCUSSION

A. FOUR MODIS LST PRODUCTS

Four products of MODIS LST at 1:00 AM, 10:00 AM, 1:00 PM, and 10:00 PM hours are utilized to model the temperature image of the earth's surface hourly in a one-year time series, i.e., total of 1460 MODIS LST images where each image covers the entire study region. Note that for the Yazd-Ardakan plain, the actual acquisition times of MODIS LST products are very close to 10:00 AM/PM (for Terra) and 1:00 AM/PM (for Aqua). Due to the drastic change in the temperature of the earth's surface, especially in desert areas, it is crucial to obtain the hourly image of LST. In Fig. 3, four MODIS LST products at different hours are illustrated, showing significant variations.

The LST changes are compared in four MODIS products. At 1:00 AM, 30% of the study region, which mostly includes highlands and mountainous areas, has LST less than 1°C, and at this hour, 95% of the study region has LST less than 6°C. At 10:00 AM, for 88% of the study region, LST is estimated to be more than 20°C, which has changed a lot compared to 1:00 AM. Between 10:00 AM and 1:00 PM, the biggest area change is related to temperatures over 30°C. In the time interval from 10:00 AM to 1:00 PM, 15% of the region of the temperature category 30-35°C is reduced and 35% is added to the area of the temperature category of more than 35°C, which indicates a sharp increase in temperature during these hours. At 10:00 PM, which is an average of 4 hours after sunset, the temperature has dropped sharply and in 58% of the study region, it is less than 6°C. The comparison of LST between 10:00 PM and 1:00 AM shows that the temperature change between these two hours is less compared to LST changes during the day. Also, the changes in LST in one pixel during one year are checked, and the amount of changes in each product is compared with each other (Fig. 4).

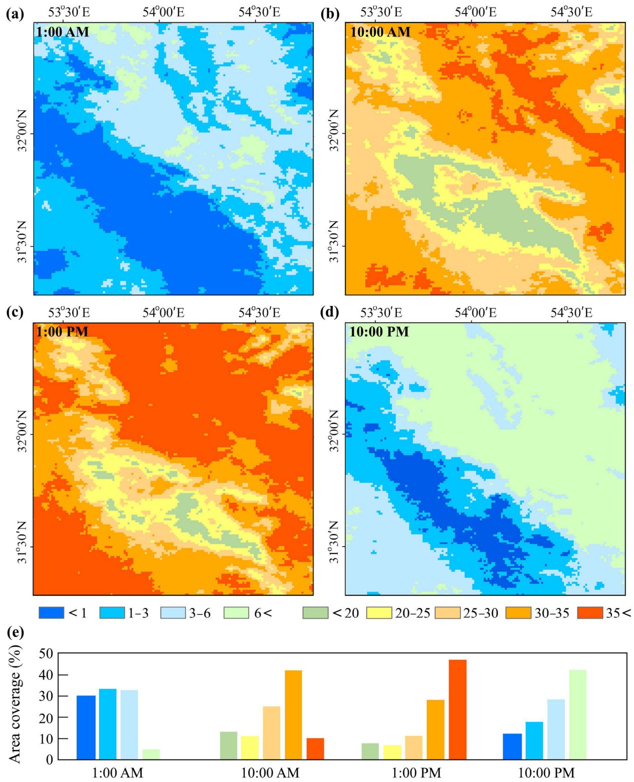

FIGURE 3. MODIS LST (°C), a) 1:00 AM, b) 10:00 AM, c) 1:00 PM, and d) 10:00 PM, e) Comparison of the floor percentage area coverage of MODIS LST at 1:00 AM, 10:00 AM, 1:00 PM, and 10:00 PM.

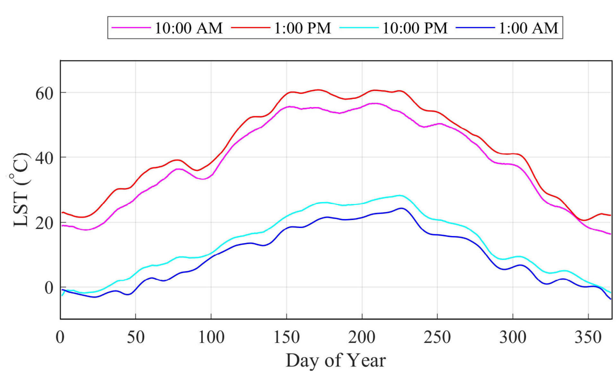

FIGURE 4. Comparison of LST (°C) in four MODIS products in a one-year time series at the scale of one pixel.

B. COMPARISON OF DTC MODELS

The LST imagery for all hours of the day and night in a one-year time series are estimated using the six DTC models. Four MODIS LST products per day, geographical coordinates, and day of the year are used as inputs for the DTC models. A MATLAB script is prepared to calculate the hourly images of the LST obtained from different methods with these inputs. First, the range and average images for each day are calculated using the four MODIS LST products. Using the images of average, range and coefficients that are mentioned in the previous section, LST is calculated hourly. The results of different models in one pixel and in one day of summer are illustrated in Fig. 5. Note that the LST starting time in Fig. 5 is at sunrise.

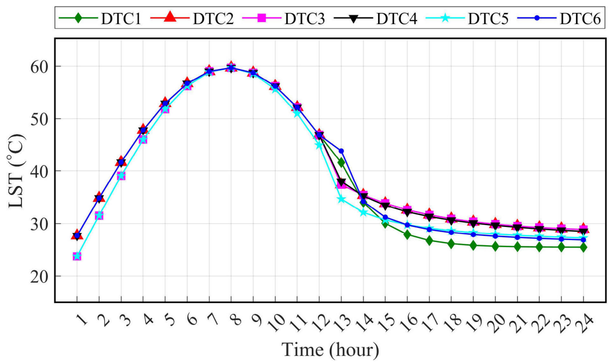

FIGURE 5. A comparison of the results of the six DTC models (°C) in one pixel and in one day of summer.

The DTC models consist of two parts of calculating the temperature before and after sunset. In some models, one of these parts is the same and the other part is calculated by a different method. Therefore, the numbers of LST calculated using different methods overlap with each other at some hours. In DTC1, DTC2, DTC4, and DTC6, the LST at sunrise and the first hour of the day is estimated at 27.7°C while in DTC3 and DTC5, it is estimated at 23.7°C. The LST at sunset is 41.6°C in DTC1, 37.4°C in the DTC2 and DTC3, and 38, 34.6, and 43.8°C in DTC4, DTC5, and DTC6, respectively. In DTC6, LST at sunset is estimated higher than other models, and the decrease in LST is more severe than in other models one hour after sunset. The lowest LST in a day and night is related to the time before sunrise, estimated as 25.5, 28.8, 28.8, 28.5, 27.2, and 26.9°C for DTC1 to DTC6, respectively. Using MODIS images, the results show that the estimated values of hourly LST are different for different models. The maximum daily temperature is the same in all models, and LST at sunrise in different models differs by 4°C. It also varies by 9°C and 3°C at sunset and before sunrise in different models, respectively. With identical inputs, different models have estimated different LST at different hours. Therefore, it is necessary to validate and use the appropriate model with the highest precision. Note that this comparison is made at the scale of one pixel.

C. COMPARISON OF DTC MODELS WITH MODIS LST PRODUCTS AT FOUR DIFFERENT HOURS

For a better and more comprehensive comparison, the MODIS LST images at 1:00 AM, 10:00 AM, 1:00 PM, and 10:00 PM are compared with the LST images obtained by different DTC models (Fig. 6). From Fig. 6, one can observe that LST in mountainous areas is generally lower than LST in plain areas, see Fig. 1. The DTC2 has the most difference from MODIS at 1:00 AM. In DTC2, more than 30% of the region is in the temperature category of higher than 22°C, while in the MODIS image at 1:00 AM, 4% of the region show a temperature higher than 22°C. In DTC2, it is assumed that there is a difference between LST at the time of sunrise and LST at the time before sunrise the next day. Therefore, in DTC2, LST at 1:00 AM, when the temperature decreases, is estimated higher than the actual value. The DTC3 and DTC4 show exactly the same results in this watch, that is why they are displayed together. In these two models, the LST region of the category above 22°C is 23% more than the one in the MODIS LST image. The DTC5 image also has a significant difference with the MODIS LST image and the temperature in this model is estimated higher than the values of MODIS. Therefore, 58% of the region has a temperature of higher than 18°C, while in the images 38% of the region is in this temperature category. This method also estimates LST at 1:00 AM higher than the actual value. The DTC6 and DTC5 are more similar to the MODIS LST at 1:00 AM. In the MODIS LST image, the largest area corresponds to the category 16 to 18°C, but in DTC6, the largest area belongs to the category 18 to 20°C. The DTC1 classes are more similar to the ones in the MODIS LST image. In DTC1, the area of the temperature categories below 10°C and above 22°C are estimated more and less than the values in MODIS LST, respectively. In general, DTC2, DTC3, DTC4, DTC5, DTC6 and DTC1, have, respectively, lowest to the highest similarity to MODIS LST at 1:00 AM.

The MODIS LST image at 10:00 AM and the six DTC models are also compared with each other (Fig. 7). The DTC1, DTC2, DTC3, DTC4, and DTC6 have estimated similar values for the temperature at 10:00 AM, and so they are displayed in one single image. Since parameter w in the DTC5 is calculated by a different method, this model estimates different LST than other models at 10:00 AM. The DTC1 to DTC4 and DTC6, LST is estimated to be lower than MODIS LST, so that the area of LST category of above 56°C is 4.2% in these models but 10.2% for MODIS, while DTC5 has estimated LST higher than other DTC models. In DTC5, the area of the temperature category of 54-56°C is 19.8% while this area is 16.1% in the MODIS LST image. In general, DTC5 is more different from the MODIS LST image at 10:00 AM, and comparing the area of the LST categories, the results of other models are closer to the MODIS product.

The LST estimated via the different DTC models has the same results at 1:00 PM, and their results are compared with the MODIS product at this time (Fig. 8). From Fig. 8, the LST

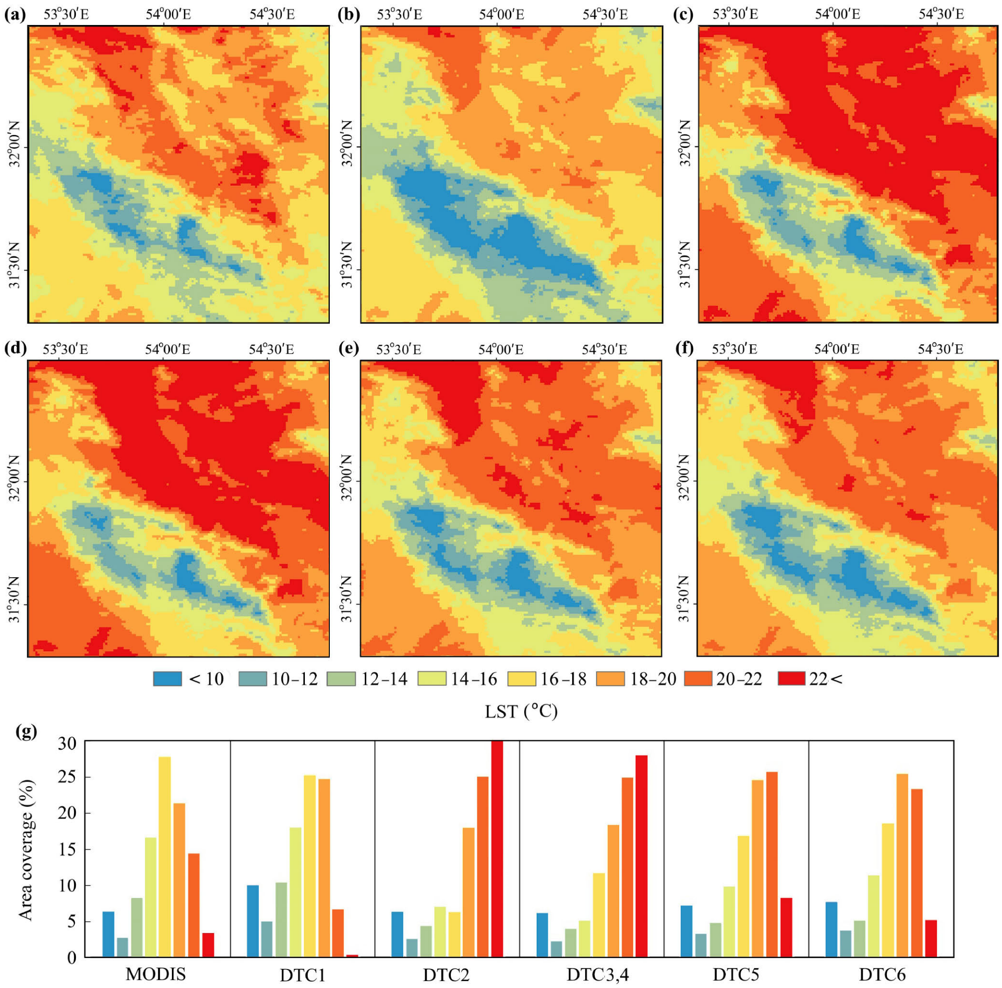

FIGURE 6. The LST images at 1:00 AM (°C): a) MODIS, b) DTC1, c) DTC2, d) DTC3,4, e) DTC5, f) DTC6, and g) Comparison of the area of the MODIS LST categories and the DTC models at 1:00 AM.

of the category above 58°C covers 29% of the study region, while in the MODIS LST image, the area of this category is 22.5%.

Finally, the LST obtained from the different DTC models at 10:00 PM are also compared with the MODIS LST image (Fig. 9). In DTC2 and DTC3, the temperature calculation algorithm is the same in the decreasing slope of the day and night temperature. For this reason, these two methods have similar results and are displayed together. The LST of DTC2 and DTC3 is more different from the MODIS LST than other models. In DTC2 and DTC3, 42% of the study region show a surface temperature of above 24°C, while in the MODIS image, this area is about 3.5%. The DTC4 has also estimated the LST in the category of above 26°C by 9% more than MODIS. Therefore, DTC2, DTC3 and DTC4 have the most difference with the MODIS product at 10:00 PM. The DTC5 and DTC6 have also estimated LST higher than the MODIS LST image for some categories. In these models, respectively, 48.5% and 42.5% of the study region has a temperature above 22°C, while in the MODIS image, this area is 23%. The DTC1 has the most similarity with MODIS. In DTC1 and MODIS LST, 23% and 21.5% of the study region is above 22°C, respectively. In order words, the LST obtained from DTC1, DTC6, DTC5, DTC4, DTC2,3 show the most to the least similarity with the MODIS product at 10:00 PM.

D. COMPARISON OF DTC MODELS IN MOUNTAIN AND PLAIN LOCATIONS IN ONE DAY

To compare the six DTC models in different lands, two locations are selected in the mountain and plain lands, see Fig. 10(a). One day in summer is chosen to compare the day-to-day changes in LST, Fig. 10(b). At 10:00 AM in the plain land, the temperature is above 50°C, and in the mountain land, the surface temperature is below 30°C. Therefore, at the same time in the study region, there is a difference of about 20°C between different land types. The LST at 1:00 AM, 10:00 AM, 1:00 PM, and 10:00 PM obtained from MODIS is also displayed on the diagram of DTC in Fig. 10(b).

The results show that the maximum LST in mountain and plain lands is 39.2 and 60°C, respectively. In other words,

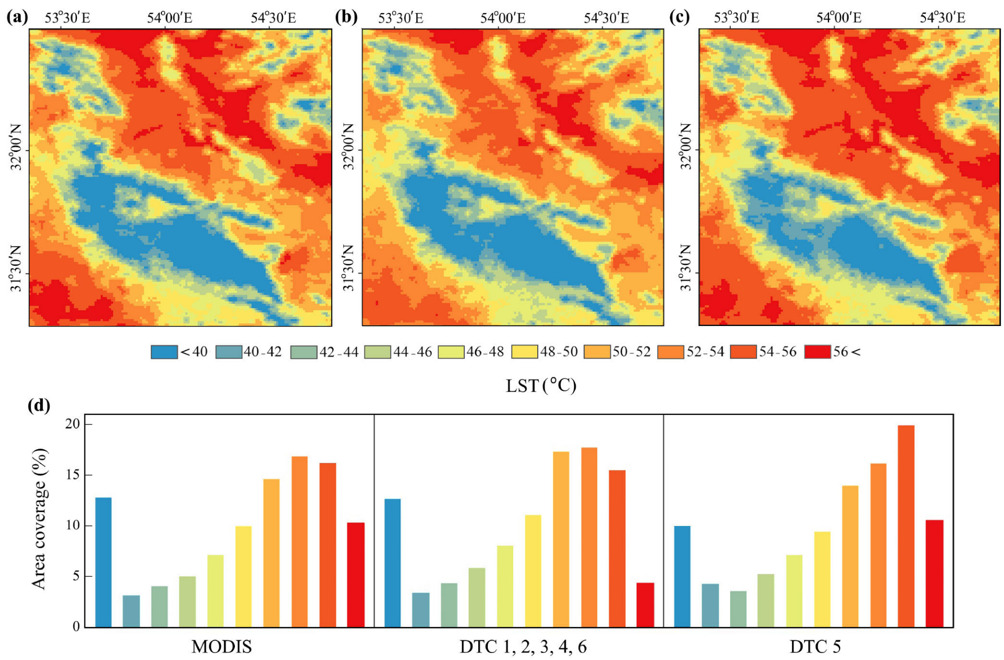

FIGURE 7. The LST images at 10:00 AM (°C): a) MODIS, b) DTC1,2,3,4,6, c) DTC5, and d) Comparison of the area of the MODIS LST categories and the DTC models at 10:00 AM.

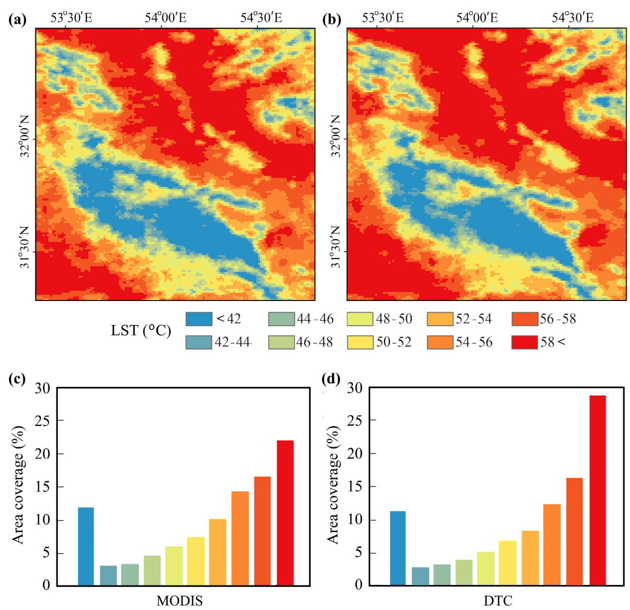

FIGURE 8. The LST images (°C) at 1:00 PM: a) MODIS, b) DTC1-6, and the area coverage (%) of the LST categories for c) MODIS, and d) DTC1-6 at 1:00 PM.

there is a difference of 20°C between the maximum LST in mountain and plain lands. The difference between the LST in mountain and plain lands is greater at the time of the maximum temperature than at other hours of the day and night. At 10:00 AM, the difference between LST in the mountain and the plain lands is 18°C. The difference in LST in the mountain and plain lands at night has decreased, so that the difference between 1:00 PM and 10:00 PM is estimated to be around 10°C, i.e., LST at 1:00 PM is 15.3°C in the mountain land and 25°C in the plain land. The range of changes in LST in one day and night is estimated to be 20°C in mountain lands and 30°C in plain lands. In addition, the average LST during the day and night is 26.2°C in the mountain lands and 40°C in the plain lands, showing the difference of 14°C in the average LST in these lands. In general, the results show that the LST changes in one day and night are more in the plain lands than in the mountain lands, and the maximum temperature difference between the plain and mountain lands is during the peak temperature hours and at the local noon time while the minimum is at night.

E. COMPARISON OF DTC MODELS IN TWO DAYS OF WINTER AND SUMMER IN ONE LOCATION

The DTC models are compared at one place in two times of the cold and warm seasons of the year (Fig. 11). The day length, times of sunrise, sunset, noon, and the MODIS LST images as inputs of the DTC models are different on these two dates, causing significant changes in the estimated LST. In winter, the maximum LST 6 hours after sunrise is 20°C and in summer 8 hours after the sunrise, it is estimated to be 56.4°C. Sunrise time is calculated at 6:00 AM in summer and 5:00 AM in winter. Note that the policies related to moving the clock forward and backward are not considered in this phase of the study. The length of the day, which determines the width of the peak and sharp drop in temperature, is estimated to be 10 hours in winter and 13 hours in summer. Therefore,

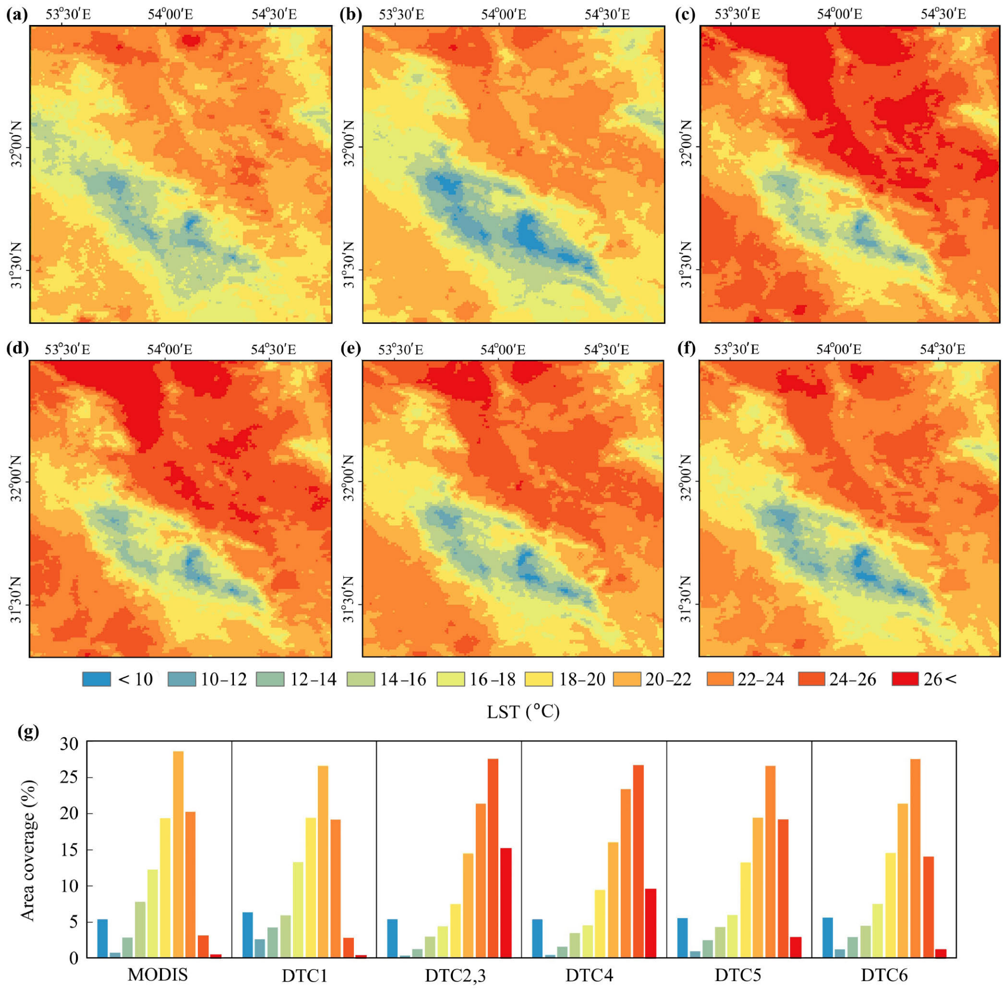

FIGURE 9. The LST images at 10:00 PM (°C): a) MODIS, b) DTC1, c) DTC2,3 d) DTC4, e) DTC5, f) DTC6, and g) Comparison of the area of the MODIS LST categories and the DTC models at 10:00 PM.

accurate estimation of sunrise, sunset, day length, etc. is very important for modeling the LST cycle. Considering that the study region is located in the hot and arid belt of the Earth and the salient features of desert areas are the large difference in day and night temperatures, the results of this section also show that the difference in the LST between day and night in summer is much greater than in winter, so that the difference in LST at noon and midnight in the warm season of the year is estimated as 33.3°C and in the cold season as 20°C. In desert areas, the main factor of soil formation and physical destruction of rocks is the large difference in day and night temperatures.

F. VALIDATION OF DTC MODELS BY GROUND MEASUREMENTS

Validation is the most important part of remote sensing studies, because the modeling is not reliable without evaluating the accuracy of the product. Using a thermometer with the ability to measure temperature with the required sequences, LST is measured in several consecutive days. However, the low spatial resolution of MODIS images and single-point temperature measurement are challenging in ground data-based validation [9]. Therefore, considering that the study region is located in the arid belt of the Earth and has desert conditions, the areas that have homogeneous land cover in a large area and about a few pixels of the MODIS image are selected for validation. As an example of such validation, a one-day real and modeled (DTC) measurements are shown in Fig. 12. Dry areas with land covers, bare lands, Hamada, barren lands and vast deserts without any cover are very suitable for validating the surface temperature and solving the problem of mixed pixels [9]. The validation results based on ground data also show that DTC1, DTC6, DTC5, DTC4, DTC3 and DTC2 have, respectively, the highest to lowest accuracy in modeling the LST diurnal cycle.

Validation is also done by comparing the hourly LST from different DTC models with hourly air temperatures acquired at an automated meteorological station. The LST is not measured in weather stations of the National Meteorological Department and in the automatic weather station used in

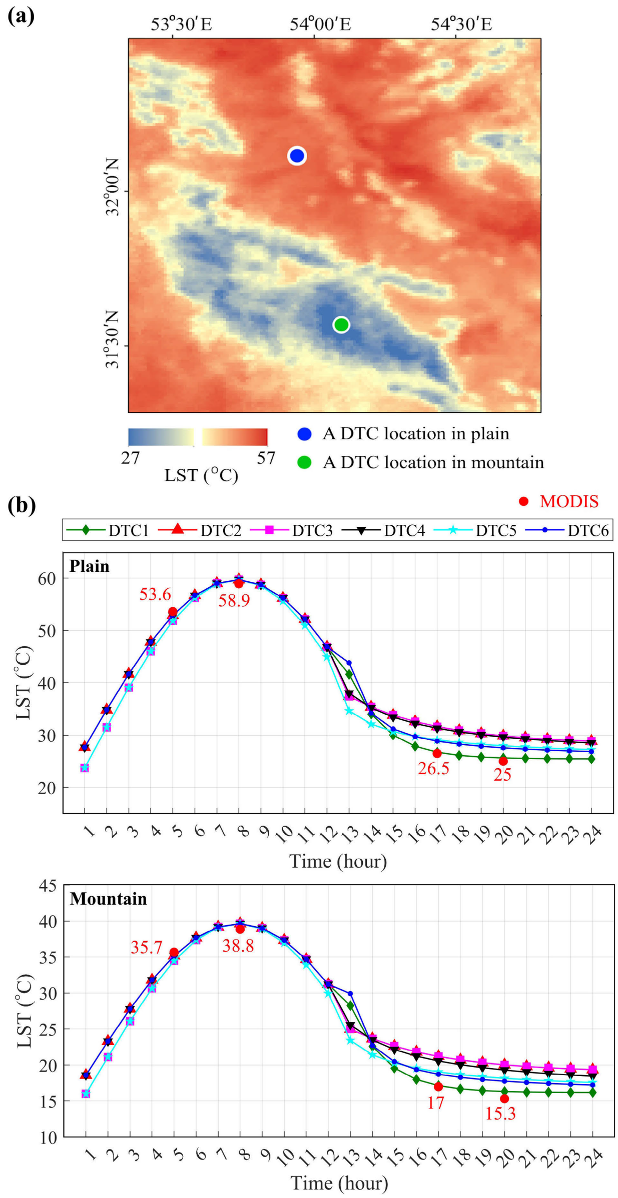

FIGURE 10. **(a) The mountain and plain locations for comparing DTC models at 10:00 AM, and (b) The LST comparison from DTC models and MODIS.**

this research, and only hourly air temperature information is available. Therefore, the hourly temperature estimated using different DTC models is compared with the hourly air temperature, air humidity percentage, and wind speed in two days of the year in summer and winter, see Fig. 13.

The automated weather station used is located on the edge of the Abarkouh desert (Latitude 31°15′9″ N and Longitude 53°43′56″ E), which has high air and LST due to its proximity to the desert. For a better comparison, one day in summer and one day in winter are selected. In general, LST is much higher than the temperature of the air, so that the maximum surface temperature of the selected hot day is 58°C and the maximum air temperature at the same time is 34.4°C. In the comparison between LST and air temperature in the summer season,

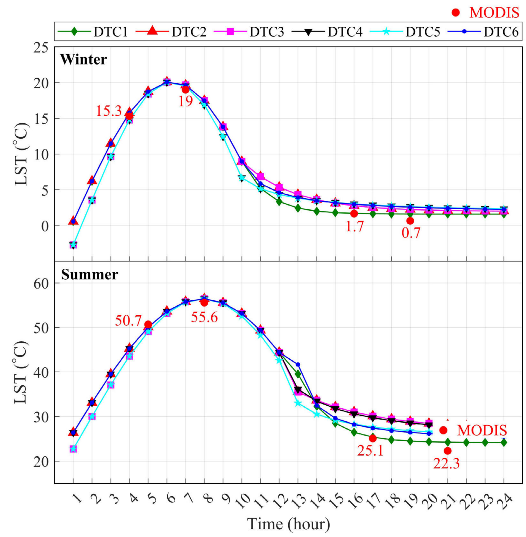

FIGURE 11. **Comparison of DTC and MODIS LST (°C) at one place in winter (top panel) and summer (bottom panel).**

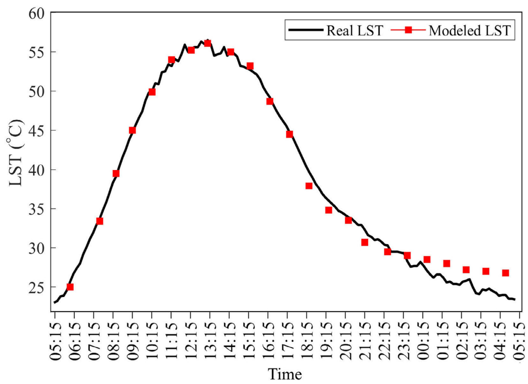

FIGURE 12. **Validation by ground measurements. The sampling intervals for the real and modeled LST are 10 minutes and 1 hour, respectively. The DTC1 is also used here.**

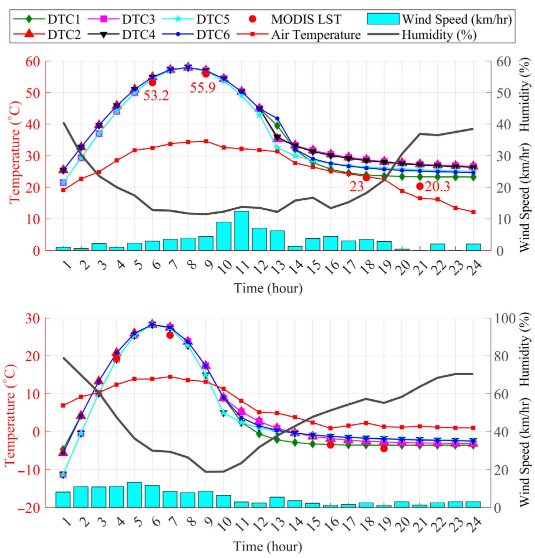

FIGURE 13. **Comparison of LST (°C) resulting from different DTC models and components of air temperature, humidity percentage, and wind speed in a hot day (top panel) and a cold day of the year (bottom panel).**

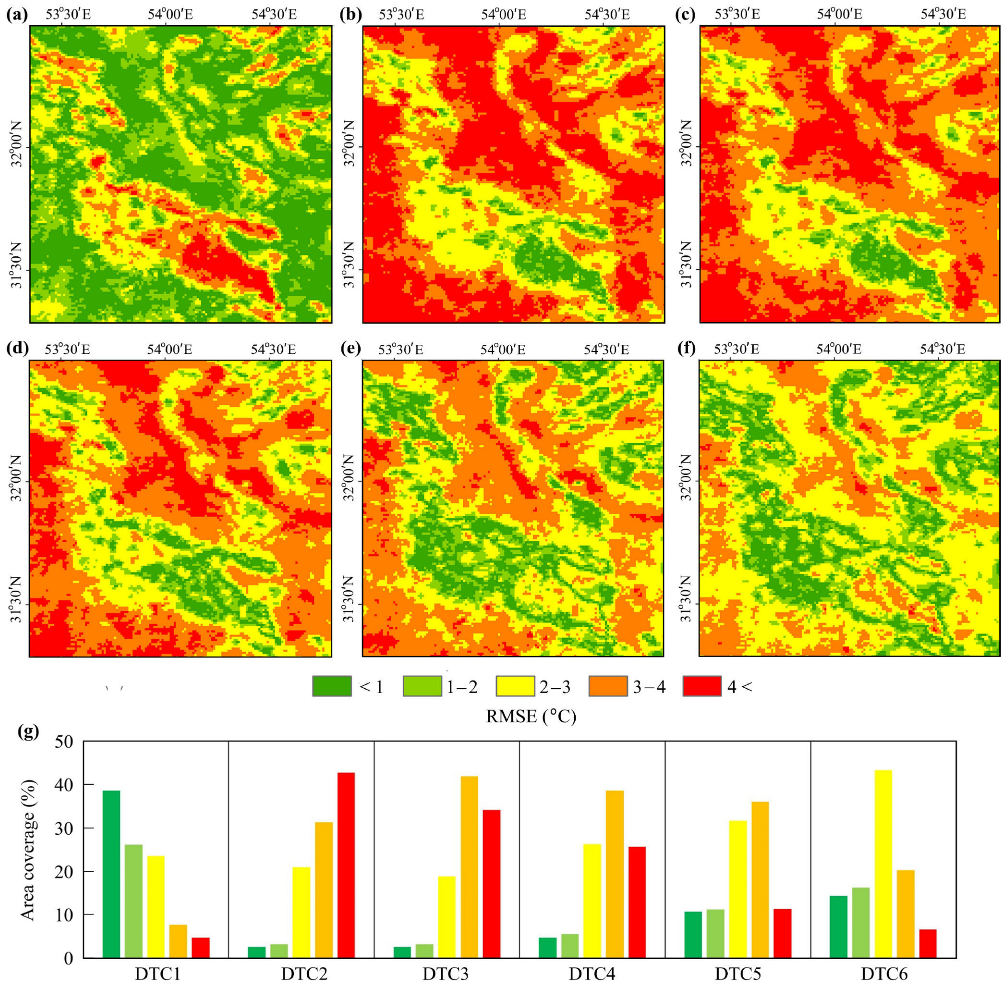

FIGURE 14. RMSE image (°C) resulting from the validation of different methods of modeling the LST diurnal cycle: a) DTC1 b) DTC2 c) DTC3 d) DTC4 e) DTC5 and f) DTC6 g) Comparison of the percentage area of the RMSE image categories.

around 3 to 5 hours after sunset, LST and air temperature are almost the same. The air temperature on the two study days clearly show an inverse relationship with air humidity percentage and wind speed, while the LST pattern did not match with wind speed and humidity percentage. It can be seen that the air temperature decreases with the increase in wind speed and humidity and vice versa.

G. VALIDATION OF DTC MODELS BY MODIS PRODUCTS

The six DTC models for a one-year time series are evaluated by MODIS LST images. Using different DTC models, hourly images of the LST are prepared in one year. For cross-validation, these images are compared with MODIS LST images at 1:00 AM, 10:00 AM, 1:00 PM, and 10:00 PM. Finally, using this comparison in one year and evaluating 4 images in each day of the year, the RMSE images of each DTC model are prepared and shown in Fig. 14. These images are the result of cross-validation and comparison of 4 modeled LST images using different DTC models and MODIS products at those times. Because the goal is select the best DTC models in estimating the LST at all hours of the day and night, accuracy assessment is not done separately for day and night.

The RMSE results show that DTC2 has the highest error. In this method, 73% of the area is covered by RMSE error greater than 3°C. Of this value, more than 42% of the area is covered by RMSE greater than 4°C. In DTC2, it is assumed that the difference between LST before sunrise and the coldest LST at night is zero, i.e., δ_T is not considered. DTC3 and DTC4 have also shown little accuracy following this method. In DTC3, 34% and in DTC4, 25% of the study region is covered by the RMSE error greater than 4°C. DTC5 is more accurate than DTC2, DTC3, and DTC4 and less accurate than the DTC6 and DTC1. In DTC5, 11% of the study region is covered by RMSE error of greater than 4°C. DTC6 and DTC1 are more accurate than other methods. In DTC6, 6% and DTC1, 4% of the region has RMSE error greater than 4°C. In DTC1, most of the area (38%) has RMSE error smaller than 1°C, and in the DTC6, the error category 2-3°C accounts for the largest area with 43%. In DTC1, 64% of the study

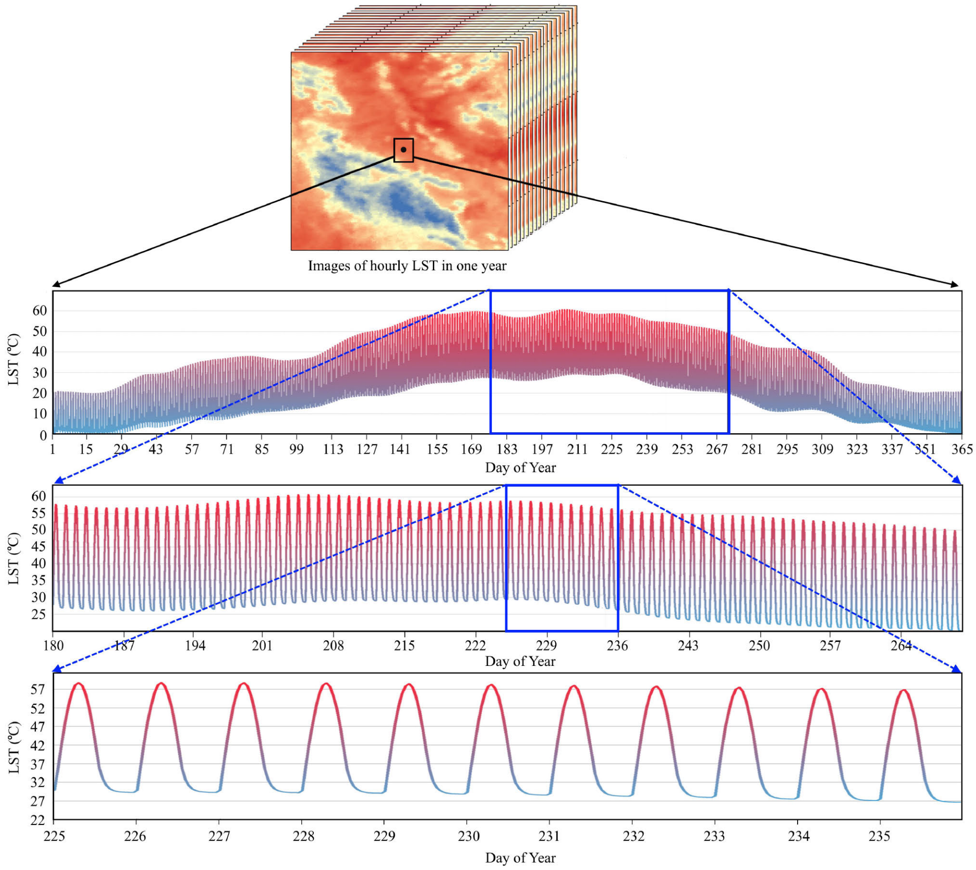

FIGURE 15. Monitoring LST hourly in a one-year time series: a) schematic image of the location of the investigated place and hourly images of the LST in one year, b) hourly examination of LST in one year, c) a magnified view in a season, and d) a magnified view of the hourly changes of the LST in 11 days.

region show RMSE error of smaller than 2°C, while the area of this category in DTC6 is 30%.

In general, the cross-validation results show that DTC1, DTC6, DTC5, DTC4, DTC3 and DTC2, respectively, show the highest to lowest accuracy in modeling the LST diurnal cycle. These results are consistent with the results in [40] and [44]. The results of estimating the average daily temperature are also consistent with the results presented in [49]. Also, the results of the present study are consistent with the findings of Coops et al. [39] who investigated the differences in morning and afternoon LST estimates from Terra and Aqua satellites in a wide range of categories, places and dates of land cover in Canada. The results show that there is a statistically significant difference between LST in the morning and in the afternoon, which varies from 0.3 to 2.3°C, depending on the type of land cover, and from 1.2 to 5°C, depending on the time of the year.

H. HOURLY LST IMAGERY IN ONE YEAR

Using different validation datasets, it is shown that DTC1 has the highest accuracy for modeling LST, and so the hourly LST images in for the year 2020 are produced by this model, illustrated in Fig. 15. An an example, one pixel is selected, and its hourly time series is also displayed in Fig. 15.

IV. CONCLUSION

In this paper, the modeling of the LST cycle was carried out using four MODIS LST images, and the hourly LST images were prepared for one year for Yazd-Ardakan plain. Six DTC models were compared and their LST results were examined by cross-validation using MODIS LST products at 1:00 AM, 10:00 AM, 1:00 PM, and 10:00 PM. The DTC models were also validated by ground measurements. It was shown that DTC1 performs better than other models for LST estimation in the arid regions. Future direction would be to investigate the possibility of modeling the LST diurnal cycle using UAV images.

COMPUTER CODE

The MATLAB code developed for this research is available online at https://github.com/Fahimearabi.

ACKNOWLEDGMENT

The authors would like to thank the NASA scientists and personnel for providing the MODIS imagery utilized in this research.

REFERENCES

[1] P. Dash, F.-M. Göttsche, F.-S. Olesen, and H. Fischer, "Land Surface Temperature and emissivity estimation from passive sensor data: Theory and practice-current trends," *Int. J. Remote Sens.*, vol. 23, no. 13, pp. 2563–2594, Jan. 2002.

[2] B. Scarino, P. Minnis, R. Palikonda, R. Reichle, D. Morstad, C. Yost, B. Shan, and Q. Liu, ''Retrieving clear-sky surface skin temperature for numerical weather prediction applications from geostationary satellite data,'' *Remote Sens.*, vol. 5, no. 1, pp. 342–366, Jan. 2013.

[3] A.-R. Cho and M.-S. Suh, ''Evaluation of Land Surface Temperature operationally retrieved from Korean geostationary satellite (COMS) data,'' *Remote Sens.*, vol. 5, no. 8, pp. 3951–3970, Aug. 2013.

[4] Q. Zhang, N. Wang, Y. Wu, and A. Chen, ''Adapting an existing empirical algorithm for microwave Land Surface Temperature retrieval in China for AMSR2 data,'' *Remote Sens.*, vol. 15, no. 13, p. 3228, Jun. 2023.

[5] M. R. Ahmed, E. Ghaderpour, A. Gupta, A. Dewan, and Q. K. Hassan, ''Opportunities and challenges of spaceborne sensors in delineating Land Surface Temperature trends: A review,'' *IEEE Sensors J.*, vol. 23, no. 7, pp. 6460–6472, Apr. 2023.

[6] A. Ignatov and G. Gutman, ''Monthly mean diurnal cycles in surface temperatures over land for global climate studies,'' *J. Climate*, vol. 12, no. 7, pp. 1900–1910, Jul. 1999.

[7] R. R. Nemani and S. W. Running, ''Estimation of regional surface resistance to evapotranspiration from NDVI and thermal-IR AVHRR data,'' *J. Appl. Meteorol.*, vol. 28, no. 4, pp. 276–284, Apr. 1989.

[8] P. K. Musyimi, G. Sahbeni, G. Timár, T. Weidinger, and B. Székely, ''Analysis of short-term drought episodes using Sentinel-3 SLSTR data under a semi-arid climate in lower eastern Kenya,'' *Remote Sens.*, vol. 15, no. 12, p. 3041, Jun. 2023.

[9] F. A. Aliabad, M. Zare, H. G. Malamiri, and E. Ghaderpour, ''Improving the accuracy of Landsat 8 Land Surface Temperature in arid regions by MODIS water vapor imagery,'' *Atmosphere*, vol. 14, no. 10, p. 1589, Oct. 2023.

[10] J. C. Price, ''Thermal inertia mapping: A new view of the Earth,'' *J. Geophys. Res.*, vol. 82, no. 18, pp. 2582–2590, Jun. 1977.

[11] W. Zhan, Y. Chen, J. Voogt, J. Zhou, J. Wang, W. Liu, and W. Ma, ''Interpolating diurnal surface temperatures of an urban facet using sporadic thermal observations,'' *Building Environ.*, vol. 57, pp. 239–252, Nov. 2012.

[12] J. Zhou, Y. Chen, X. Zhang, and W. Zhan, ''Modelling the diurnal variations of urban heat islands with multi-source satellite data,'' *Int. J. Remote Sens.*, vol. 34, no. 21, pp. 7568–7588, Nov. 2013.

[13] I. Keramitsoglou, C. T. Kiranoudis, and Q. Weng, ''Downscaling geostationary Land Surface Temperature imagery for urban analysis,'' *IEEE Geosci. Remote Sens. Lett.*, vol. 10, no. 5, pp. 1253–1257, Sep. 2013.

[14] W. Zhan, J. Zhou, W. Ju, M. Li, I. Sandholt, J. Voogt, and C. Yu, ''Remotely sensed soil temperatures beneath snow-free skin-surface using thermal observations from tandem polar-orbiting satellites: An analytical three-time-scale model,'' *Remote Sens. Environ.*, vol. 143, pp. 1–14, Mar. 2014.

[15] J. Lu, L. Jia, C. Zheng, R. Tang, and Y. Jiang, ''A scheme to estimate diurnal cycle of evapotranspiration from geostationary Meteorological Satellite observations,'' *Water*, vol. 12, no. 9, p. 2369, 2020.

[16] C. L. Errea, C. R. D. Almeida, A. Gonçalves, and A. C. Teodoro, ''Remote sensing analysis of the surface urban heat island effect in Vitoria–Gasteiz, 1985 to 2021,'' *Remote Sens.*, vol. 15, no. 12, p. 3110, Jun. 2023.

[17] F. Aires, C. Prigent, and W. B. Rossow, ''Temporal interpolation of global surface skin temperature diurnal cycle over land under clear and cloudy conditions,'' *J. Geophys. Res., Atmos.*, vol. 109, no. D4, pp. 1–18, Feb. 2004.

[18] R. T. Pinker, D. Sun, M. Miller, and G. J. Robinson, ''Diurnal cycle of Land Surface Temperature in a desert encroachment zone as observed from satellites,'' *Geophys. Res. Lett.*, vol. 34, no. 11, pp. 1–5, Jun. 2007.

[19] Q. Weng and P. Fu, ''Modeling diurnal land temperature cycles over Los Angeles using downscaled GOES imagery,'' *ISPRS J. Photogramm. Remote Sens.*, vol. 97, pp. 78–88, Nov. 2014.

[20] Z. Liu, P. Wu, S. Duan, W. Zhan, X. Ma, and Y. Wu, ''Spatiotemporal reconstruction of Land Surface Temperature derived from FengYun geostationary satellite data,'' *IEEE J. Sel. Topics Appl. Earth Observ. Remote Sens.*, vol. 10, no. 10, pp. 4531–4543, Oct. 2017.

[21] C. O. Justice, J. R. G. Townshend, E. F. Vermote, E. Masuoka, R. E. Wolfe, N. Saleous, D. P. Roy, and J. T. Morisette, ''An overview of MODIS land data processing and product status,'' *Remote Sens. Environ.*, vol. 83, nos. 1–2, pp. 3–15, Nov. 2002.

[22] S. Shiff, D. Helman, and I. M. Lensky, ''Worldwide continuous gap-filled MODIS Land Surface Temperature dataset,'' *Sci. Data*, vol. 8, no. 1, p. 74, Mar. 2021.

[23] D. J. Mildrexler, M. Zhao, and S. W. Running, ''A global comparison between station air temperatures and MODIS Land Surface Temperatures reveals the cooling role of forests,'' *J. Geophys. Res.*, vol. 116, no. G3, pp. 1–15, 2011.

[24] H. Xia, Y. Chen, A. Gong, K. Li, L. Liang, and Z. Guo, ''Modeling daily temperatures via a phenology-based annual temperature cycle model,'' *IEEE J. Sel. Topics Appl. Earth Observ. Remote Sens.*, vol. 14, pp. 6219–6229, 2021.

[25] F. Zhao, C. Tang, X. Tian, X. Wu, C. Dai, and H. Wei, ''The global spatial and temporal distribution of ice cloud optical thickness based on MODIS satellite data during 2000–2021,'' *Atmosphere*, vol. 14, no. 6, p. 977, Jun. 2023.

[26] M. Shawky, M. R. Ahmed, E. Ghaderpour, A. Gupta, G. Achari, A. Dewan, and Q. K. Hassan, ''Remote sensing-derived Land Surface Temperature trends over South Asia,'' *Ecol. Informat.*, vol. 74, May 2023, Art. no. 101969.

[27] A. Reinart and M. Reinhold, ''Mapping surface temperature in large lakes with MODIS data,'' *Remote Sens. Environ.*, vol. 112, no. 2, pp. 603–611, Feb. 2008.

[28] E. Ghaderpour, P. Mazzanti, G. S. Mugnozza, and F. Bozzano, ''Coherency and phase delay analyses between land cover and climate across Italy via the least-squares wavelet software,'' *Int. J. Appl. Earth Observ. Geoinf.*, vol. 118, Apr. 2023, Art. no. 103241.

[29] A. Xie, J. Zhu, X. Qin, and S. Wang, ''The Antarctic amplification based on MODIS Land Surface Temperature and ERA5,'' *Remote Sens.*, vol. 15, no. 14, p. 3540, Jul. 2023.

[30] S.-B. Duan, Z.-L. Li, H. Li, F.-M. Göttsche, H. Wu, W. Zhao, P. Leng, X. Zhang, and C. Coll, ''Validation of collection 6 MODIS Land Surface Temperature product using in situ measurements,'' *Remote Sens. Environ.*, vol. 225, pp. 16–29, May 2019.

[31] Y. Zhang, X. Li, K. Zhang, L. Wang, S. Cheng, and P. Song, ''A simple real LST reconstruction method combining thermal infrared and microwave remote sensing based on temperature conservation,'' *Remote Sens.*, vol. 15, no. 12, p. 3033, Jun. 2023.

[32] F. Hong, W. Zhan, F.-M. Göttsche, Z. Liu, J. Zhou, F. Huang, J. Lai, and M. Li, ''Comprehensive assessment of four-parameter diurnal Land Surface Temperature cycle models under clear-sky,'' *ISPRS J. Photogramm. Remote Sens.*, vol. 142, pp. 190–204, Aug. 2018.

[33] M. Jin and R. E. Dickinson, ''Interpolation of surface radiative temperature measured from polar orbiting satellites to a diurnal cycle: 1. Without clouds,'' *J. Geophys. Res., Atmos.*, vol. 104, no. D2, pp. 2105–2116, Jan. 1999.

[34] D. Sun and R. T. Pinker, ''Implementation of GOES-based Land Surface Temperature diurnal cycle to AVHRR,'' *Int. J. Remote Sens.*, vol. 26, no. 18, pp. 3975–3984, Sep. 2005.

[35] F. Huang, W. Zhan, S.-B. Duan, W. Ju, and J. Quan, ''A generic framework for modeling diurnal Land Surface Temperatures with remotely sensed thermal observations under clear sky,'' *Remote Sens. Environ.*, vol. 150, pp. 140–151, Jul. 2014.

[36] M. Gholamnia, S. K. Alavipanah, A. D. Boloorani, S. Hamzeh, and M. Kiavarz, ''Diurnal air temperature modeling based on the Land Surface Temperature,'' *Remote Sens.*, vol. 9, no. 9, p. 915, Sep. 2017.

[37] P. Hu, A. Wang, Y. Yang, X. Pan, X. Hu, Y. Chen, X. Kong, Y. Bao, X. Meng, and Y. Dai, ''Spatiotemporal downscaling method of Land Surface Temperature based on daily change model of temperature,'' *IEEE J. Sel. Topics Appl. Earth Observ. Remote Sens.*, vol. 15, pp. 8360–8377, 2022.

[38] F.-M. Göttsche and F. S. Olesen, ''Modelling of diurnal cycles of brightness temperature extracted from METEOSAT data,'' *Remote Sens. Environ.*, vol. 76, no. 3, pp. 337–348, Jun. 2001.

[39] N. C. Coops, D. C. Duro, M. A. Wulder, and T. Han, ''Estimating afternoon MODIS Land Surface Temperatures (LST) based on morning MODIS overpass, location and elevation information,'' *Int. J. Remote Sens.*, vol. 28, no. 10, pp. 2391–2396, May 2007.

[40] S.-B. Duan, Z.-L. Li, N. Wang, H. Wu, and B.-H. Tang, ''Evaluation of six land-surface diurnal temperature cycle models using clear-sky in situ and satellite data,'' *Remote Sens. Environ.*, vol. 124, pp. 15–25, Sep. 2012.

[41] T. R. H. Holmes, W. T. Crow, and C. Hain, ''Spatial patterns in timing of the diurnal temperature cycle,'' *Hydrol. Earth Syst. Sci.*, vol. 17, no. 10, pp. 3695–3706, 2013.

[42] S.-B. Duan, Z.-L. Li, B.-H. Tang, H. Wu, R. Tang, Y. Bi, and G. Zhou, ''Estimation of diurnal cycle of Land Surface Temperature at high temporal and spatial resolution from clear-sky MODIS data,'' *Remote Sens.*, vol. 6, no. 4, pp. 3247–3262, Apr. 2014.

[43] Y. Malbéteau, S. Parkes, B. Aragon, J. Rosas, and M. McCabe, ''Capturing the diurnal cycle of Land Surface Temperature using an unmanned aerial vehicle,'' *Remote Sens.*, vol. 10, no. 9, p. 1407, Sep. 2018.

[44] C. Nie, J. Liao, G. Shen, and W. Duan, ''Simulation of the Land Surface Temperature from Moon-based Earth observations,'' *Adv. Space Res.*, vol. 63, no. 2, pp. 826–839, Jan. 2019.

[45] Y. Chang, Y. Ding, Q. Zhao, and S. Zhang, ''A comprehensive evaluation of 4-parameter diurnal temperature cycle models with in situ and MODIS LST over Alpine meadows in the Tibetan Plateau,'' *Remote Sens.*, vol. 12, no. 1, p. 103, Dec. 2019.

[46] Z. Sharifnezhadazizi, H. Norouzi, S. Prakash, C. Beale, and R. Khanbilvardi, ''A global analysis of Land Surface Temperature diurnal cycle using MODIS observations,'' *J. Appl. Meteorol. Climatol.*, vol. 58, no. 6, pp. 1279–1291, Jun. 2019.

[47] A. Sekertekin, N. Arslan, and M. Bilgili, ''Modeling diurnal Land Surface Temperature on a local scale of an arid environment using artificial neural network (ANN) and time series of Landsat-8 derived spectral indexes,'' *J. Atmos. Solar-Terrestrial Phys.*, vol. 206, Sep. 2020, Art. no. 105328.

[48] L. Hu, Y. Sun, G. Collins, and P. Fu, ''Improved estimates of monthly Land Surface Temperature from MODIS using a diurnal temperature cycle (DTC) model,'' *ISPRS J. Photogramm. Remote Sens.*, vol. 168, pp. 131–140, Oct. 2020.

[49] Z. Xing, Z.-L. Li, S.-B. Duan, X. Liu, X. Zheng, P. Leng, M. Gao, X. Zhang, and G. Shang, ''Estimation of daily mean Land Surface Temperature at global scale using pairs of daytime and nighttime MODIS instantaneous observations,'' *ISPRS J. Photogramm. Remote Sens.*, vol. 178, pp. 51–67, Aug. 2021.

[50] P. Sismanidis, B. Bechtel, I. Keramitsoglou, F. Göttsche, and C. T. Kiranoudis, ''Satellite-derived quantification of the diurnal and annual dynamics of Land Surface Temperature,'' *Remote Sens. Environ.*, vol. 265, Nov. 2021, Art. no. 112642.

[51] L. Lu and X. M. Zhou, ''A four-parameter model for estimating diurnal temperature cycle from MODIS Land Surface Temperature product,'' *J. Geophys. Res., Atmos.*, vol. 126, no. 8, pp. 1–18, Apr. 2021, Art. no. e2020JD033855.

[52] A. Jia, S. Liang, and D. Wang, ''Generating a 2-km, all-sky, hourly Land Surface Temperature product from advanced baseline imager data,'' *Remote Sens. Environ.*, vol. 278, Sep. 2022, Art. no. 113105.

[53] F. Hong, W. Zhan, F.-M. Göttsche, Z. Liu, P. Dong, H. Fu, F. Huang, and X. Zhang, ''A global dataset of spatiotemporally seamless daily mean Land Surface Temperatures: Generation, validation, and analysis,'' *Earth Syst. Sci. Data*, vol. 14, no. 7, pp. 3091–3113, Jul. 2022.

[54] Q. Huang and Y. Lu, ''The effect of urban heat island on climate warming in the Yangtze River delta urban agglomeration in China,'' *Int. J. Environ. Res. Public Health*, vol. 12, no. 8, pp. 8773–8789, Jul. 2015.

[55] M. Wang, H. Lu, B. Chen, W. Sun, and G. Yang, ''Fine-scale analysis of the long-term urban thermal environment in Shanghai using Google Earth Engine,'' *Remote Sens.*, vol. 15, no. 15, p. 3732, Jul. 2023.

[56] A. M. El Kenawy, M. E. Hereher, and S. M. Robaa, ''An assessment of the accuracy of MODIS Land Surface Temperature over Egypt using ground-based measurements,'' *Remote Sens.*, vol. 11, no. 20, p. 2369, Oct. 2019.

[57] F. Becker and Z.-L. Li, ''Towards a local split window method over land surfaces,'' *Int. J. Remote Sens.*, vol. 11, no. 3, pp. 369–393, Mar. 1990.

[58] S. M. Jaber and M. M. Abu-Allaban, ''MODIS-based Land Surface Temperature for climate variability and change research: The tale of a typical semi-arid to arid environment,'' *Eur. J. Remote Sens.*, vol. 53, no. 1, pp. 81–90, Jan. 2020.

[59] Z. Wan and Z.-L. Li, ''A physics-based algorithm for retrieving land-surface emissivity and temperature from EOS/MODIS data,'' *IEEE Trans. Geosci. Remote Sens.*, vol. 35, no. 4, pp. 980–996, Jul. 1997.

[60] J. Tan, T. Che, J. Wang, J. Liang, Y. Zhang, and Z. Ren, ''Reconstruction of the daily MODIS Land Surface Temperature product using the two-step improved similar pixels method,'' *Remote Sens.*, vol. 13, no. 9, p. 1671, Apr. 2021.

[61] Z. Wan, ''New refinements and validation of the collection-6 MODIS Land-Surface Temperature/emissivity product,'' *Remote Sens. Environ.*, vol. 140, pp. 36–45, Jan. 2014.

[62] L. Pérez-Planells, D. Ghent, S. Ermida, M. Martin, and F.-M. Göttsche, ''Retrieval consistency between LST CCI satellite data products over Europe and Africa,'' *Remote Sens.*, vol. 15, no. 13, p. 3281, Jun. 2023.

[63] Y. Wang, J. Liu, and W. Zhu, ''Estimation of instantaneous air temperature under all-weather conditions based on MODIS products in North and Southwest China,'' *Remote Sens.*, vol. 15, no. 11, p. 2701, May 2023.

[64] F. A. Aliabad, ''Reconstructing daytime and nighttime MODIS Land Surface Temperature in desert areas using multi-channel singular spectrum analysis,'' *Adv. Space Res.*, 2024.

[65] M. Ghil, M. R. Allen, M. D. Dettinger, K. Ide, D. Kondrashov, M. E. Mann, A. W. Robertson, A. Saunders, Y. Tian, F. Varadi, and P. Yiou, ''Advanced spectral methods for climatic time series,'' *Rev. Geophys.*, vol. 40, no. 1, p. 1003, Feb. 2002.

[66] W. J. Parton and J. A. Logan, ''A model for diurnal variation in soil and air temperature,'' *Agricult. Meteorol.*, vol. 23, pp. 205–216, Jan. 1981.

[67] A. Ruzmaikin, H. H. Aumann, J. Lee, and J. Susskind, ''Diurnal cycle variability of surface temperature inferred from AIRS data,'' *J. Geophys. Res., Atmos.*, vol. 122, no. 20, pp. 928–938, Oct. 2017.

[68] R. Khandan, M. Gholamnia, S.-B. Duan, M. Ghadimi, and S. K. Alavipanah, ''Characterization of maximum Land Surface Temperatures in 16 years from MODIS in Iran,'' *Environ. Earth Sci.*, vol. 77, no. 12, p. 450, Jun. 2018.

[69] S.-B. Duan, Z.-L. Li, H. Wu, B.-H. Tang, X. Jiang, and G. Zhou, ''Modeling of day-to-day temporal progression of clear-sky Land Surface Temperature,'' *IEEE Geosci. Remote Sens. Lett.*, vol. 10, no. 5, pp. 1050–1054, Sep. 2013.

[70] Y. Yamamoto, K. Ichii, Y. Ryu, M. Kang, S. Murayama, S.-J. Kim, and J. R. Cleverly, ''Detection of vegetation drying signals using diurnal variation of Land Surface Temperature: Application to the 2018 East Asia heatwave,'' *Remote Sens. Environ.*, vol. 291, Jun. 2023, Art. no. 113572.

[71] S. B. Idso, R. D. Jackson, and R. J. Reginato, ''Compensating for environmental variability in the thermal inertia approach to remote sensing of soil moisture,'' *J. Appl. Meteorol.*, vol. 15, no. 8, pp. 811–817, Aug. 1976.

[72] J. D. Lin, ''On the force-restore method for prediction of ground surface temperature,'' *J. Geophys. Res., Oceans*, vol. 85, no. C6, pp. 3251–3254, Jun. 1980.

[73] N. A. Elagib, S. H. Alvi, and M. G. Mansell, ''Day-length and extraterrestrial radiation for Sudan: A comparative study,'' *Int. J. Sol. Energy*, vol. 20, no. 2, pp. 93–109, 1999.

[74] P. I. Cooper, ''The absorption of radiation in solar stills,'' *Sol. Energy*, vol. 12, no. 3, pp. 333–346, 1969.

[75] S. Schädlich, ''Influence of land surface parameters and atmosphere on METEOSAT brightness temperatures and generation of Land Surface Temperature maps by temporally and spatially interpolating atmospheric correction,'' *Remote Sens. Environ.*, vol. 75, no. 1, pp. 39–46, Jan. 2001.

[76] F. Van den Bergh, M. A. van Wyk, B. J. van Wyk, and G. Udahemuka, ''A comparison of data-driven and model-driven approaches to brightness temperature diurnal cycle interpolation,'' *SAIEE Afr. Res. J.*, vol. 98, no. 3, pp. 81–86, Sep. 2007.

[77] A. K. Inamdar and A. French, ''Disaggregation of GOES land surface temperatures using surface emissivity,'' *Geophys. Res. Lett.*, vol. 36, no. 2, pp. 1–5, Jan. 2009.

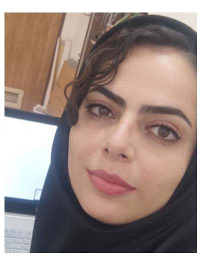

FAHIME ARABI ALIABAD received the bachelor's degree in natural resources engineering and the M.Sc. and Ph.D. degrees in the management of dry and desert areas from Yazd University, Iran, in 2015, 2017, and 2023, respectively. She is conducting research in remote sensing with Yazd University. She is doing research on precision agriculture issues using drones, testing stress, identifying weeds and separating different species, estimating soil depth temperature using satellite images, and gap filling of surface temperature images. She has won the Award of the Best Researcher of the master's degree and doctoral level of Yazd University, in 2016 and 2020, respectively.

EBRAHIM GHADERPOUR received the first Ph.D. degree in theoretical and computational science from the University of Lethbridge, Canada, in 2013, and the second Ph.D. degree in remote sensing from York University, Canada, in 2018. He is an Assistant Professor of remote sensing with the Department of Earth Sciences, Sapienza University of Rome, Italy. He completed two postdoctoral appointments with the University of Calgary, Canada. He is also the CEO of Earth and Space Inc., Calgary, Canada. His research interest revolves around big data analytics and artificial intelligence, with their applications in remote sensing, geology, geosciences, robotics, and medicine. He is an academic editor and a reviewer of many journals.

MOHAMMAD ZARE received the Ph.D. degree in desertification from Ghent University, Belgium, in 2008. He started his career with the Geography Department, Yazd University, Iran, where he is an Associate Professor of environmental and desert studies with the Department of Arid Lands Management. His research interests include desertification, land degradation, soil and water conservation, and soil conservation. He is an Editor of the *Journal of Arid Land Management*.

HAMIDREZA GHAFARIAN MALAMIRI received the B.Sc. degree in soil and water engineering from Tehran University, Iran, the M.Sc. degree in geomatics engineering from Twente University, The Netherlands, and the Ph.D. degree in remote sensing from Delft University of Technology, in 2015. He started his career with the Geography Department, Yazd University, Iran. He became the Chair of the Geography Department, Yazd University, in 2018, and the Deputy Head of education and research with the Faculty of Humanities and Social Science, in 2020. He is an Associate Professor of remote sensing and GIS with Yazd University. His research interests focus on remote sensing, GIS, and spatial and spatio-temporal data, such as monitoring data, thermal remote sensing, time series analysis, and others.

Open Access funding provided by ‘Università degli Studi di Roma "La Sapienza" 2’ within the CRUI CARE Agreement